Eur. Phys. J. A **5**, 327–336 (1999)

THE EUROPEAN PHYSICAL JOURNAL A

Hydrogen doppler spectroscopy using ^{15}N ions*

L. Borucki, H.W. Becker, F. Gorris, S. Kubsky, W.H. Schulte, C. Rolfs

Institut für Physik mit Ionenstrahlen, Ruhr-Universität Bochum, Bochum, Germany

Received: 1 March 1999
Communicated by B. Povh

Abstract. The energy spread of atomic and molecular ion beams from the 4 MV Dynamitron tandem accelerator at the Ruhr-Universität Bochum has been studied and in part minimized. Using the $E_R = 6.40$ MeV narrow resonance in ^{1}H(^{15}N,$\alpha\gamma$)^{12}C with an ^{15}N energy spread of 4.55 keV, the Doppler broadening for several hydrogen-bearing gases was found to be in good agreement with expectation: e.g. for NH_3 gas a rotational-vibrational Doppler width of 10.41 ± 0.25 keV was observed (theory = 10.4 keV). Studies of the vibrational Doppler widths of H-bonds on a Si $\langle 100 \rangle$ surface were performed using a 4π γ-ray detection system together with UHV-chambers for sample preparation, transport, and analysis. The results showed that further improvements in the experimental set-ups are needed for such investigations.

1 Introduction

Ion beams play an important role in materials science, especially in the chemical analysis of samples [1–3]. Hydrogen is of high importance: it is a common contaminant in nearly all samples, it is often contained in the surface layers of a sample, and it can have dramatic effects on the chemical, physical, and electrical properties of many materials, particularly of thin films. Ion beam techniques satisfy most hydrogen analytical needs. The nuclear resonant reaction analysis (NRRA) technique is attractive and powerful because of its inherent capability of providing a non-destructive (with respect to the stoichiometry), fast, sensitive, and simple analysis of the total quantity of hydrogen and its depth distribution in a sample. The most popular NRRA technique is the $E_R = 6.400$ MeV resonance in ^{1}H(^{15}N,$\alpha\gamma$)^{12}C (width $\Gamma_R = 1.44$ keV, strength $\omega\gamma = 21.1$ eV [4]), in short "^{15}N-technique". The resonance parameters allow a H-detection sensitivity in the 10 ppm range and a depth resolution near the sample surface of about 10 nm. Moreover, the thermal motion of the H target atoms (translation, vibration, and rotation where applicable) contributes a Gaussian broadening to the Lorentzian resonant yield curve, due to the Doppler effect. The magnitude of this Doppler broadening depends on the amplitude of the velocity component in beam direction of the moving H atoms, which in turn depends on the nature of the H-bond. Typically, a Doppler broadening of the order of $\Delta E_D = 10$ keV (FWHM) has been observed [5–11], which can be determined with high precision if the intrinsic energy spread of the ^{15}N ion beam, ΔE_B, is precisely known and significantly smaller than 10 keV. If this condition is fulfilled, the ^{15}N technique can form eventually a valuable tool for investigating the bonding characteristics of the H subsystem of samples, e.g. dangling bonds of a H-terminated Si surface.

The energy spread of a ^{15}N ion beam from a tandem accelerator can have many sources: e.g. ion source spread, high voltage ripple, energy straggling and Coulomb explosion in the stripper gas. To elucidate these sources, we have studied [12] – in a first step – the simplest atomic ion beam, i.e. protons: we investigated its energy spread over the high voltage range $U_{HV} = 0.2$ to 3.4 MV of the 4 MV Dynamitron tandem accelerator. In a second step, the energy spread was measured for heavier negatively charged atomic ion beams as well as for negatively charged molecular ion beams, such as needed for the ^{15}N-technique. In a third step, the Doppler broadening was measured for several hydrogen-bearing gases using the ^{15}N-technique, followed by measurements of H-bonds on a Si surface.

2 Energy spread of proton beams

Details of the 4 MV Dynamitron tandem accelerator at the Ruhr-Universität Bochum have been described previously [4, 13, 14]. In all experiments described below, the width of the object slits of the analysing magnet was set at 0.81 mm and the width of the image slits at $\Delta x = 1.52$ mm, if not quoted differently. At these slit widths, nearly the full proton beam current from the ion source was available at the target location. The energy resolution of the analysing magnet is given by the equation $\Delta E = E\Delta x/R$, where E is

* Supported in part by the Deutsche Forschungsgemeinschaft (Ro 429/24)

the beam energy and R = 653 mm is the bending radius of the magnet (e.g. ΔE = 1.15 keV for E = 500 keV and Δx = 1.52 mm). Similar techniques as before [4, 14] have been used in preliminary experiments, such as thick-target yield curves for the narrow E_R = 992 keV resonance in ^{27}Al(p,γ)^{28}Si (Γ_R = 70 eV [15]) and automatic energy scanning. In contrast to [4], the HV-ripple due to the 115 kHz oscillator (producing the high voltage of the tandem) could be minimized in the present work by moving a new balance plate to an appropriate position. In this position, the contribution of the 115 kHz ripple to the overall energy spread was found to be ΔE_B(115 kHz) $\approx$ 90 eV at U_{HV} = 450 kV. The position with minimal ripple was found to be independent of the high voltage of the tandem: using the narrow E_R = 1748 keV resonance in ^{13}C(p,γ)^{14}N (Γ_R = 145 eV [16]), the minimum position was unchanged and the observed spread was here ΔE_B(115 kHz) $\approx$ 180 eV at U_{HV} = 830 kV, indicating a nearly linear increase with high voltage. An influence on the energy spread due to other periodic frequencies – such as the line frequency (50 Hz) and its harmonics – has not been found. Finally, a kryo pump located near the object slits of the analysing magnet could cause non-periodic vibrations of the slits: however, there were no noticeable changes in the ΔE_B values when the kryo pump was switched off for a short time.

For detailed measurements of the energy spread, a windowless gas target system with five pumping stages was used [4]. Briefly, the beam entered a disc-shaped target chamber through six apertures of high gas flow impedance and was stopped in a Faraday cup 3 m from the center of the chamber. The chamber had several ports radiating from its center, which was at a distance of 105 mm from the entrance aperture. These ports were used for several purposes, such as gas-inlet, pressure measurement, and installation of a Si surface barrier detector. The gas pressure in the target chamber, p_0, was measured with a capacitance manometer to an accuracy of 4%. This measurement was absolute and independent of the gas used. The Si detector (active area = 280 mm^2, thickness = 100 μm, energy resolution = 19 keV at E_α = 5 MeV) was installed at the 30° port of the target chamber. The detector was collimated with a tube of 10 mm inner diameter and 130 mm length, with a central collimator (4.0 mm diameter) at the end facing the detector. The distance from the collimator to the center of the target chamber was 230 mm. This geometry defined the effective target length seen by the detector as 35.4 mm, corresponding to an angular range of the observed ejectiles between θ_{lab} = 27.8° and 32.3°. The elastic scattering yield observed in the Si detector was used to monitor the product of beam intensity and target density. For γ-ray spectroscopy, a 4"×4" BGO crystal was placed in close geometry at a distance (to its front end) of 20 mm from the beam axis. The lead shielding around the crystal defined the effective target length seen by the crystal to 105 mm for a 4.4 MeV γ-ray (^{15}N-technique).

With this setup, excitation curves were obtained for the narrow resonance in ^{22}Ne(p,γ)^{23}Na at E_R = 948 keV (Γ_R = 29 eV [15]) as a function of gas pressure

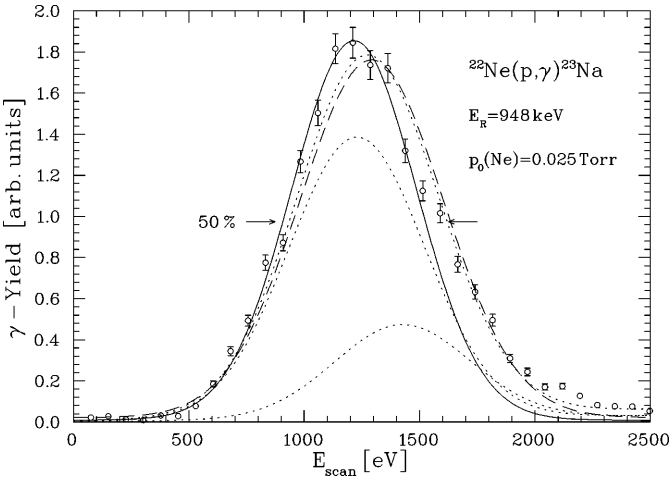

Fig. 1. Excitation function of the γ-ray yield emitted by the E_R = 948 keV resonance in ^{22}Ne(p,γ)^{23}Na at a neon gas pressure of p_0 = 0.025 Torr. The energy variation E_{scan} was carried out using an energy scanning technique [14]. The dashed curve represents a fit using one Voigt function, while the dotted curves (and their sum) represent a fit using two Voigt functions shifted by 210 eV (due to concurrent atomic excitations). The solid curve represents one Voigt function fitted only to the low-energy edge of the excitation function

p_0 (using neon gas of natural isotopic composition containing 10% ^{22}Ne). The resonant γ-ray flux was normalized to the concurrently observed elastic scattering flux, which follows the Rutherford scattering law at this energy and scattering angle. An excitation function obtained at p_0(Ne) = 0.025 Torr is shown in Fig. 1. In a first step, the width of the yield curve was extracted from the 50% yield points at the low-energy and high-energy edges: $\Delta E_{exp}(p_0) = 728 \pm 60$ eV. In a second step, the excitation function has been described by a Voigt function, which represents the convolution of a Lorentzian distribution and a Gaussian distribution. The Lorentzian distribution is characterized by the resonance width Γ_R (Table 1) and the width of the Gaussian distribution contains in quadratures the beam energy spread, the energy straggling in the gas (ΔE_S), and the Doppler width: $\Delta E_{exp}(p_0) = (\Delta E_B^2 + \Delta E_S(p_0)^2 + \Delta E_D^2)^{1/2} = 719 \pm 26$ eV (dashed curve in Fig. 1). Furthermore, for single collision conditions concurrent atomic excitations in the nuclear collision (i.e. for zero impact parameter) can lead to observable replica resonances at energies above E_R [18]. For a proton beam of 948 keV one expects mainly an excitation of the atomic L-shell in the compound atom Na, with a probability of P(L) = 29 ± 4% and a mean energy shift of $Q_m = 180 \pm 30$ eV [12]. Thus, the data have been fitted – in a third step – with two Voigt functions (with the same Gaussian width (ΔE_{exp}) separated by the energy Q_m and scaled by P(L), where both Q_m and P(L) have been varied within the uncertainties quoted above. The best fit led (dotted curves in Fig. 1) to the parameters $\Delta E_{exp}(p_0) = 665 \pm 21$ eV, Q_m = 210 eV, and P(L) = 29%. Since the quantities Q_m and P(X) for other resonance

Table 1. Energy spread ΔE_B of ion beams deduced from narrow resonances

Reaction	E_R[a] (keV)	Γ_R[a] (eV)	ΔE_{DT}[g] (eV)	Beam[h] IN	Beam[h] OUT	U_{HV} (MV)	ΔE_{exp}[i] (eV)	ΔE_B[j] (eV)	E_C[m] (eV)
proton beams									
^{22}Ne(p,γ)^{23}Na	479[b]	21[c]	78	H^-	H^+	0.19	568±14	563±14	
^{22}Ne(p,γ)^{23}Na	638[b]	65[b]	90	H^-	H^+	0.27	610±9	603±9	
^{22}Ne(p,γ)^{23}Na	851[b]	6[b]	104	H^-	H^+	0.38	658±8	650±8	
^{22}Ne(p,γ)^{23}Na	948[b]	29[b]	110	H^-	H^+	0.43	626±8	618±8	
^{22}Ne(p,γ)^{23}Na	1278[b]	69[b]	128	H^-	H^+	0.59	649±13	636±13	
^{22}Ne(p,γ)^{23}Na	1721[b]	25[b]	148	H^-	H^+	0.82	764±25	750±25	
^{20}Ne(p,γ)^{21}Na	3552[b]	455d	223	H^-	H^+	1.73	1127±90	1104±90	
^{20}Ne(p,γ)^{21}Na	6872[b]	402d	311	H^-	H^+	3.39	1520±82	1489±82	
atomic negative ion beams									
^{4}He(^{7}Li,γ)^{11}B	1425e	5e	839	Li^-	Li^+	0.67	1550±43	693±85	
^{4}He(^{11}B,γ)^{15}N	1666f	9f	1134	B^-	B^+	0.79	2090±270	≤1140	
^{4}He(^{16}O,γ)^{20}Ne	5270e	140e	2433	O^-	O^{2+}	1.73	4750±780	1880±800[k]	
molecular negative ion beams									
^{22}Ne(p,γ)^{23}Na	948[b]	29[b]	110	OH^-	H^+	0.89	1509±74	1327±77[l]	1.61±0.18
^{22}Ne(p,γ)^{23}Na	1721[b]	25[b]	148	OH^-	H^+	1.62	1976±160	1745±165[l]	1.53±0.28
^{4}He(^{7}Li,γ)^{11}B	1425e	5e	839	LiO^-	Li^+	1.09	2980±430	2526±436[l]	1.25±0.44
^{4}He(^{11}B,γ)^{15}N	1666f	9f	1134	B_2^-	B^+	1.06	2700±180	1433±215[l]	0.35±0.10
^{4}He(^{14}N,γ)^{18}F	5663e	590e	2360	CN^-	N^{2+}	2.20	7999±640	4687±442[kl]	1.81±0.34
^{4}He(^{14}N,γ)^{18}F	5663e	590e	2360	NH_2^-	N^{2+}	1.92	6514±180	3554±166[kl]	2.70±0.25[n]
^{4}He(^{14}N,γ)^{18}F	5663e	590e	2360	NH^-	N^{2+}	1.90	6010±500	3130±350[kl]	3.8±0.8
^{4}He(^{16}O,γ)^{20}Ne	5270e	140e	2433	OH^-	O^{2+}	1.76	6210±1070	3014±1086[kl]	4.2±2.0

[a] In the laboratory system [b] From [15] [c] From calculations of the penetrability, assuming a reduced proton width of $\Theta^2 = 0.01$ [d] Present work (appendix) [e] From [16] [f] From [17] [g] Translational Doppler broadening for T = 294 K [h] Ion beam before the high voltage terminal (IN) and after the analysing magnet (OUT) [i] Observed energy spread extrapolated to zero gas pressure; the quoted error includes a 1.1% uncertainty in the energy scanning system [j] Observed energy spread (column 8) corrected for the contribution of the Doppler width (column 4). The observed spreads are significantly smaller than the energy resolution of the analysing magnet (Sect. 2). [k] Corrected for the $2/(1+q)$ scaling according to [4] (here: 2/3 for q = 2) [l] Energy spread ΔE_{CE} due to Coulomb explosion [m] Coulomb energy involved in the molecular breakup [n] Assuming a breakup into the bicluster N plus H_2

studies are not known with sufficient precision, we have fitted – in a fourth step – only the low-energy edge of the excitation function with one Voigt function, minimizing thus the contributions of replica resonances to the observed energy spread: the resulting value of $\Delta E_{exp}(p_0) = 625 \pm 13$ eV (solid curve in Fig. 1) is in fair agreement with the above value including atomic excitations. We have followed the procedure of this fourth step in the analysis of all data.

The width $\Delta E_{exp}(p_0)$ as a function of po, shown in Fig. 2, reaches an asymptotic value at low pressure. The extrapolated value at zero pressure is then independent of energy loss and energy straggling effects in the target gas: $\Delta E_{exp}(p_0 = 0) = \Delta E_{exp} = (\Delta E_B^2 + \Delta E_D^2)^{1/2} = 626 \pm 8$ eV (Table 1). Since the neon gas has only translational degrees of freedom, the Doppler width ΔE_{DT} at the resonance energy E_R is given by the expression [19]

$$\Delta E_D = \Delta E_{DT} = 4(\ln 2\, M_p M_t^{-1} E_R kT)^{1/2}, \qquad (1)$$

where M_p and M_t are the masses of projectiles and target nuclides, respectively, and T is the gas temperature. With $\Delta E_{DT} = 110$ eV (at $E_R = 948$ keV and T = 294 K), one arrives at an energy spread of $\Delta E_B = 618 \pm 8$ eV (Table 1).

A similar procedure applied to the narrow resonances in ^{22}Ne(p,γ)^{23}Na at E_R = 479, 638, 851, 1278, and 1721 keV [15] led to results summarized in Table 1. For the resonances in ^{20}Ne(p,γ)^{21}Na at E_R = 3552 and 6872 keV, respective total widths of $\Gamma_R \approx 400$ and ≤1200 eV have been reported [15]; the actual respective values are $\Gamma_R = 455 \pm 67$ and 402 ± 60 eV (appendix).

The ΔE_B values for the neon resonances (Table 1) are displayed in Fig. 3 and have been parametrized by the quadratic addition of a constant term, $\Delta E_c = 599 \pm 6$ eV, and a term increasing linearly with high voltage U_{HV}. The linearly increasing term should arise from the HV-ripple scaling with the high voltage, consistent with the ΔE_B(115 kHz) results quoted above. To test this conclusion, the contribution of the 115 kHz ripple to the energy spread was measured using the E_R = 948 keV resonance in ^{22}Ne(p,γ)^{23}Na (U_{HV} = 0.42 MV) and a technique described in [14]. Briefly, the proton energy was set at the 50% low-energy yield point of the thick-target excitation function. Further, a time-to-amplitude (TAC) converter

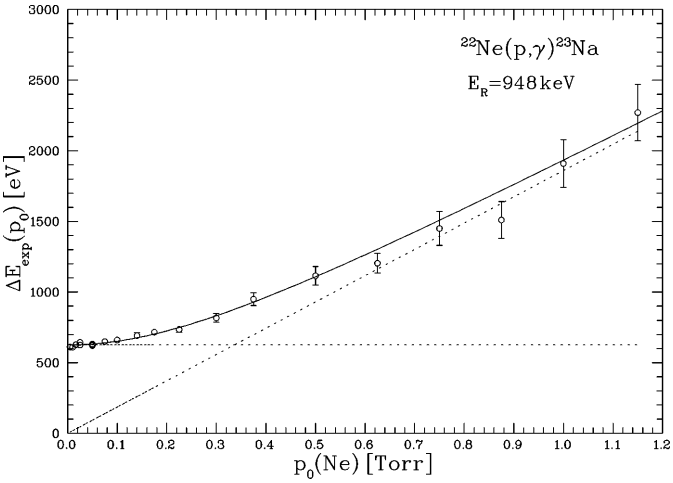

Fig. 2. Energy spread $\Delta E_{exp}(p_0)$ as a function of neon gas pressure p_0, extracted from excitation functions of the γ-ray yield emitted by the E_R = 948 keV resonance in $^{22}Ne(p,\gamma)^{23}Na$. The data are described (solid curve) by the quadratic addition of a constant term, $\Delta E(p_0) = 626 \pm 8$ eV, and a term increasing linearly with pressure (dotted lines)

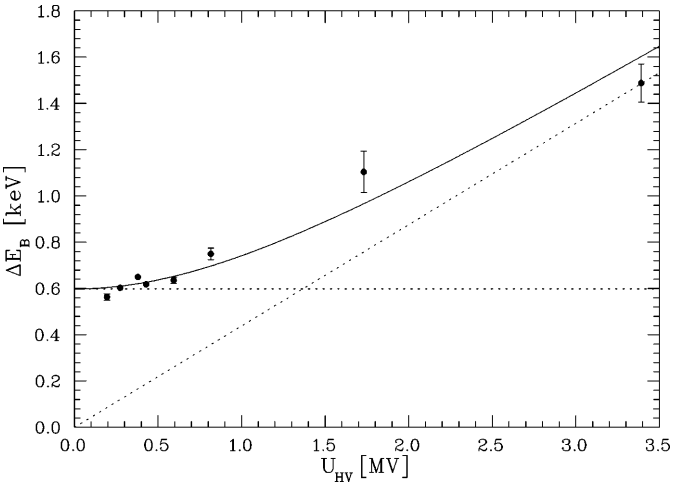

Fig. 3. Energy spread ΔE_B of protons as a function of high voltage U_{HV}. The data are described (solid curve) by the quadratic addition of a constant term and a term increasing linearly with high voltage (dotted lines)

was used, where the start signal was provided by the zero crossing of the 115 kHz frequency (= 8.7 μs) and the stop signal by the resonant capture γ-rays. The time range of the TAC was limited to 1 μs leading to a negligible observable energy variation by the HV-ripple, at the cost of a reduced useful beam intensity. The resulting value $\Delta E_B(TAC = 1\,\mu s)$ in comparison with the unlimited value $\Delta E_B(TAC = 8.7\,\mu s)$ led to $\Delta E_c(115\,kHz) = 190 \pm 20$ eV at $U_{HV} = 0.42$ MV, consistent with the value of 184 eV expected from Fig. 3.

In order to elucidate the major sources of the constant term, several components of the tandem accelerator have been studied as discussed below.

The proton beam in the above experiments has been produced using a duoplasmatron (DP) ion source plus its injection system at 90 kV. In order to measure its contribution to ΔE_c, the high voltage of the accelerator was turned off and the 90 keV H^--beam was guided (through the accelerator "drift" tubes) to the analysing magnet, which was used as an energy analyser. The resulting distribution was measured as a function of the width of the image slits and reached an asymptotic value $\Delta E_c(DP) \approx 200$ eV at small slit widths. This value is much larger than expected for this source system: $\Delta E_c(DP) \approx 20$ eV. Thus, additional measurements were carried out using the narrow resonance in $^{22}Ne(p,\gamma)^{23}Na$ at $E_R = 948$ keV ($p_0 = 0.025$ Torr); the proton beam was produced both by the duoplasmatron ion source and a sputter ion source (with its own injection system). The resulting widths led to an energy spread of the duoplasmatron ion source of $\Delta E_c(DP) = 280 \pm 12$ eV, in fair agreement with the value quoted above; the results indicate significant (non-harmonic) instabilities in the equipment of the duoplasmatron ion source.

The stripper gas (oxygen) in the high voltage terminal can contribute to the overall energy spread due to energy straggling in the gas. Unfortunately, the pressure in the stripper canal (tube of 126 cm length and 1 cm diameter) could not be measured directly, but only indirectly via the current of the analysed beam. This current was maximized (I_{max}) in the above experiments by variation of the gas pressure in the stripper canal. Taking the analysed current as a measure of this gas pressure, excitation functions were obtained as a function of decreasing proton current (i.e. decreasing gas pressure). The results obtained with the sputter ion source led to $\Delta E_c(STRIPPER\text{-}GAS) = 368 \pm 23$ eV at I_{max}.

The mechanical vibrations of the kryo pumps in the high voltage terminal can cause a contribution to the total energy spread. Thus, an excitation function was obtained with the kryo pumps turned off for about 10 minutes: during this time the cold faces of the pumps had still sufficient pumping speeds for the stripper gas. A comparison of the width values for the ON and OFF situations led to the (non-harmonic) contribution $\Delta E_c(KRYO) = 289 \pm 21$ eV.

Finally, the slit feedback system (SFS) of the accelerator stabilisation [4, 14] was investigated: excitation functions were obtained with the system ON and OFF, where in the OFF mode the high voltage was stabilized by the voltage given by one of the resistor chains of the accelerator. A comparison of the width values for the ON and OFF modes led to the contribution $\Delta E_c(SFS) = 206 \pm 20$ eV, indicating an (unsolved) electronic problem in the SFS.

The quadratic addition of the contributions just discussed leads to an expected total energy spread of $\Delta E_c = 583 \pm 39$ eV, in good agreement with observation (599 ± 6 eV). Thus, it is concluded that the major sources of the observed energy spread for a proton beam have been found. If future technical improvements of the duoplasmatron injection system and slit feedback system could remove their contributions to the energy spread, one will arrive at $\Delta E_c = 466$ eV. Further, replacing the kryo pumps by

turbo pumps in the HV terminal could lead to $\Delta E_c = 368$ eV, the contribution from energy straggling in the stripper gas. This contribution could also be minimized by reducing the pressure of the stripper gas, with a concurrent reduction in beam current if acceptable by the experiment (Sect. 5). A further technical minimalization of the HV-ripple (scaling linearly with high voltage, Fig. 3) appears difficult, except by the use of a TAC with limited time range (see above); the price is again a significant reduction in exploitable beam current.

3 Energy spread of atomic ion beams

The experiments just discussed involved the simplest beam, protons, with an atomic ion beam of negative charge incident onto the high voltage terminal (IN: H^-) and an atomic ion beam of selected positive charge leaving the high voltage terminal and the analysing magnet (OUT: H^+). In a second series of experiments, other atomic ion beams (IN: X^-, OUT: X^+) have been studied: ^{7}Li, ^{11}B and ^{16}O. The studies involved narrow (α, γ) resonances in inverse kinematics (He target gas). The observed energy spreads ΔE_{exp} (extrapolated to zero gas pressure) are given in Table 1. The values are significantly higher than those of protons, mainly due to a different energy straggling ΔE_S in the stripper gas. Assuming the Bohr straggling model with $\Delta E_S \approx Z_p$ (i.e., a linear scaling with the atomic number of the projectile) and an identical stripper gas pressure, the observed value $\Delta E_S(H)$ for protons (see above) leads to $\Delta E_S(Li) = 1104$ eV, $\Delta E_S(B) = 1840$ eV, and $\Delta E_S(O) = 2944$ eV. Quadratic subtraction of the contributions $\Delta E_S(X)$ and ΔE_{DT} (Table 1) from the observed ΔE_{exp} values led to energy spreads $\Delta E_B(X)$ (Table 1), in fair agreement with the corresponding values for protons. Note that the quoted value for $\Delta E_B(O)$ was corrected for the $2/(1+q)$ scaling (q = charge state of the emerging ion beam; here q = 2) according to [4].

In summary, energy straggling in the stripper gas makes the major contribution to the total energy spread of atomic ion beams, an unavoidable disadvantage of tandem accelerators.

4 Energy spread of molecular ion beams

Since the lifetime of N^- atomic ions is extremely short, the ^{15}N-technique must involve a molecular ion beam (such as CN^- or NH^-) incident on the high voltage terminal. Thus, the energy spread of several molecular ion beams (IN: XY^-, OUT: X^+) have been studied in a third series of experiments. The studies involved narrow resonances and the noble gases He and Ne, where the resonances have been initiated in inverse kinematics where applicable (Table 1).

A diatomic molecule XY^- with masses m_x and m_y (total mass $M = m_x + m_y$) and a radial distance R_M between the two atoms is accelerated to the terminal high voltage U_{HV} of the tandem. In the first few atomic layers of the stripper gas, the molecule is broken up into its atoms carrying a mean charge q_x and q_y, a process called Coulomb explosion [20]. The explosion liberates a Coulomb energy

$$E_C = q_x q_y e^2 / R_M, \tag{2}$$

which is shared by the two atomic fragments leading to an energy spread

$$\Delta E_{CE} = 4(2\ \ln 2\, m_x m_y M^{-2}\, eU_{HV} E_C)^{1/2}. \tag{3}$$

It should be pointed out that the mass dependence in equation 3 has a maximum for $m_x = m_y$, while it reaches a low value for $m_x \ll m_y$ or $m_y \ll m_x$. For the ^{15}N-technique it appears thus to be advantageous using a $^{15}NH^-$ ion beam ($m_x m_y / M^2 = 0.059$) instead of a $^{15}NC^-$ ion beam ($m_x m_y / M^2 = 0.25$), i.e. the smaller the atomic mass of the accompanying partner, the closer one reaches the limiting case of an atomic ion beam with a minimal contribution of ΔE_{CE} to the overall energy spread of the ion beam. Note also that the atomic fragments (after the Coulomb explosion) reach a charge state distribution in the stripper gas, where the charge state q of interest is selected by the experimentor.

The Coulomb energy E_C (2) depends on the mean charge state q_i, into which the atomic fragments are broken up during the Coulomb explosion. If one fragment is characterized by $q_i = 0$, then $E_C = 0$ and thus $\Delta E_{CE} = 0$. Since there exists no information on the mean charge state q_i, we extracted from the observed value ΔE_{CE} the empirical value for E_C; then, assuming a molecular radius $R_M = 1$ A°, a value for the product of the mean charge states $q_x q_y$ was deduced.

As an illustrating example, consider the case of the $E_R = 948$ keV resonance in ^{22}Ne(p,γ)^{23}Na investigated with an OH^- molecular beam (Table 1). The observed width $\Delta E_{exp} = 1509 \pm 74$ eV was corrected for the contributions of Doppler width ($\Delta E_{DT} = 110$ eV) and accelerator components ($\Delta E_B = 709 \pm 20$ eV at $U_{HV} = 0.89$ MV, Fig. 3). The result is $\Delta E_{CE} = 1327 \pm 77$ eV and thus $E_C = 1.61 \pm 0.18$ eV (Table 1) and $q_x q_y = 0.11 \pm 0.01$. Another example is the $E_R = 1425$ keV resonance in ^{4}He(^{7}Li,γ)^{11}B, with an observed width $\Delta E_{exp} = 2980 \pm 430$ eV, a Doppler width $\Delta E_{DT} = 839$ eV, an energy straggling $\Delta E_S = 1104 \pm 69$ eV (Sect. 3), and an accelerator spread $\Delta E_B = 759 \pm 25$ eV at $U_{HV} = 1.09$ MV (Fig. 3). The values lead to $\Delta E_{CE} = 2526 \pm 436$ eV and thus to $E_C = 1.25 \pm 0.44$ eV (Table 1) and $q_x q_y = 0.09 \pm 0.03$. The corresponding results for other molecular ion beams are summarized in Table 1.

The E_C values for the different systems don't vary significantly but are of the order of about 1.5 eV (Table 1) corresponding to $q_x q_y \approx 0.10$. Thus, one of the atomic fragments is – with a probability of about 90% – electrically neutral in the Coulomb explosion, i.e. the effects of the Coulomb explosion are drastically reduced; a similar observation has been reported for H-molecules fragmented in a gas target [20].

In summary, the energy spread of molecular ion beams has another significant contribution due to the Coulomb explosion of the molecule in the stripper gas.

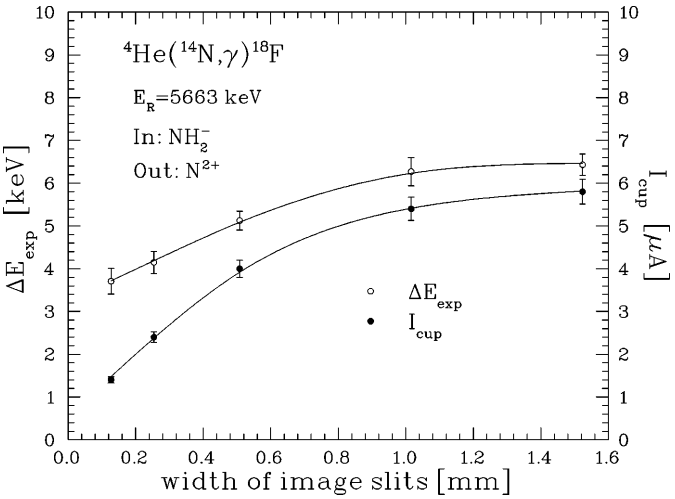

Fig. 4. Energy spread ΔE_{exp} and beam current I_{cup} are shown as a function of the width of the image slits of the analysing magnet

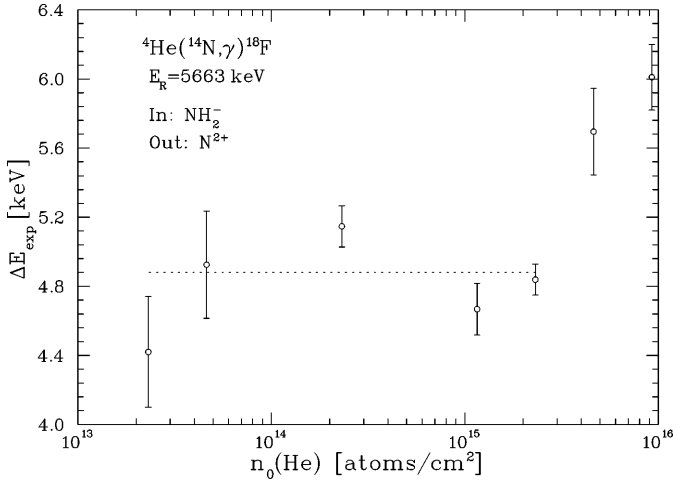

Fig. 5. Energy spread $\Delta E_{exp}(p_0)$ of the $E_R = 5663$ keV resonance in ^{4}He(^{14}N,γ)^{18}F is shown as a function of He gas density

5 Optimisation of the energy spread for the ^{15}N-technique

The ^{15}N-technique can be carried out using molecular ion beams of the type CN^-, NH_2^-, or NH^-. Using the $E_R = 5663$ keV narrow resonance in ^{4}He(^{14}N,γ)^{18}F, the energy spread of such beams was investigated. The results (Table 1) show that the total energy spread ΔE_{exp} and the contribution of the Coulomb explosion ΔE_{CE} are smallest for the NH^- ion beam, as expected from (3). While the values for a NH_2^- ion beam are only slightly larger than those of NH^-, the current of this beam is about one order of magnitude higher. We have thus restricted the next experimental step to the NH_2^- ion beam. In order to improve the total energy spread, the width of the image slits was reduced from the usual value of 1.52 mm ("brute force method"). The results for ΔE_{exp} and the resulting beam currents are shown in Fig. 4: at a slit width of 0.13 mm one finds $\Delta E_{exp} = 3.71 \pm 0.30$ keV with a reduction in beam current by a factor 4.1. As a compromise for the measurements described in Sect. 6, we have used a slit width of 0.25 mm resulting in $\Delta E_{exp} = 4.15 \pm 0.26$ keV and $\Delta E_B = 3.41 \pm 0.26$ keV at $U_{HV} = 1.92$ MV. Scaling – with (3) – the result to $U_{HV} = 2.18$ MV for the ^{15}N-technique, one finds $\Delta E_B = 3.63 \pm 0.28$ keV.

6 Doppler spectroscopy of hydrogen-bearing gases

The ^{15}N-technique was used to measure the bond-dependent Doppler broadening using several hydrogen-bearing gases: H_2, C_2H_6, CH_4, H_2O, and NH_3. These gases are well suited for this purpose in that each affords the opportunity to measure a single bond species (i.e. H-H, C-H, N-H, and O-H) without contributions from other bonds (Sect. 7). For this aim, one must measure the Doppler width due to vibrations and rotations of the gas molecule, ΔE_{DVR}. Similarly to (1), the theoretical width ΔE_{DVR} is described by the equation

$$\Delta E_{DVR} = 4(\ln 2\, M_p M_t^{-1} E_R (E_v + E_r))^{1/2}, \qquad (4)$$

where E_v and E_r are the vibrational and rotational energies of the molecule [5].

For H_2 gas with a pressure of $p_0(H_2) = 0.050$ Torr, the observed excitation function leads to $\Delta E_{exp} = 9.46 \pm 0.66$ keV. After quadratic subtraction of the contributions $\Delta E_B = 3.63$ keV and $\Delta E_{DT} = 3.67$ keV, one finds $\Delta E_{DVR}(H_2) = 7.93 \pm 0.72$ keV, in good agreement with the expected value of 7.5 keV [5]. For ethan gas (C_2H_6) at $p_0 = 0.010$ Torr one finds $\Delta E_{exp} = 12.9 \pm 3.3$ keV. With $\Delta E_{DT} = 0.95$ keV, one arrives at $\Delta E_{DVR}(C_2H_6) = 12.3 \pm 3.3$ keV, consistent with the expected value of 10.4 keV [12].

In order to improve significantly the experimental sensitivity even at a sub-monolayer target thickness and thus to reduce the experimental uncertainties in ΔE_{DVR} (see above), a 12"×12" NaI crystal in combination with a new gas target system has been used [12] (a similar setup for solid targets is shown in Fig. 7). The crystal has a central bore hole of 35 mm diameter and a 0.5 mm Al wall thickness. With a γ-ray source at the center of the crystal, the total efficiency of this 4π crystal was observed to be nearly 100% for monoenergetic γ-rays up to 10 MeV [21]. A beam pipe of 32 mm diameter and 110 cm effective length was installed in the bore hole and pumped on both sides by turbo pumps (pumping speeds = 360 and 520 l/s). The gas pressure in the pipe was measured with a Penning vacuum meter and a mass analyser. For He gas at $p_0 = 6 \times 10^{-6}$ to 1.2×10^{-3} Torr and a 110 cm target length, one finds an areal target density of $n_0 = 2.5 \times 10^{13}$ to 1×10^{16} atoms/cm^2 (i.e. about 10^{-3} to 10 monolayers).

Using the $E_R = 5663$ keV narrow resonance in ^{4}He(^{14}N,γ)^{18}F (IN: NH_2^-, OUT: N^{2+}; width of image slits = 0.25 mm), the energy spread ΔE_{exp} has been measured as a function of target density. The results (Fig. 5)

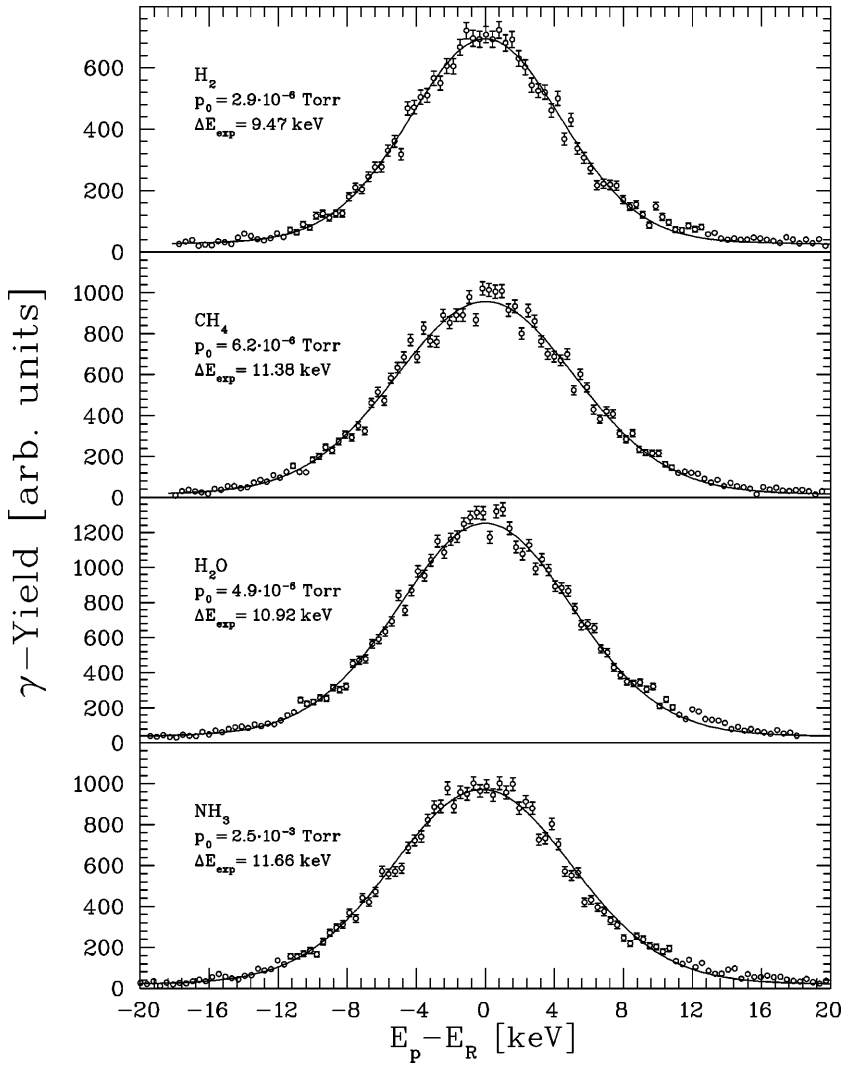

Fig. 6. Yield curves of several hydrogen-bearing gases using the ^{15}N-technique

show that ΔE_{exp} is independent of the gas density for values less or equal one monolayer, while it increases significantly above 5 monolayers. The data lead to a beam energy spread $\Delta E_B = 4.27 \pm 0.16$ keV at $U_{HV} = 1.92$ MV, somewhat higher than the value quoted above. Scaling the result to $U_{HV} = 2.18$ MV for the ^{15}N-technique, one finds $\Delta E_B = 4.55 \pm 0.17$ keV, which has been adopted in the following analyses.

For H_2 gas at $p_0 = 3.4 \times 10^{-7}$ to 1.5×10^{-5} Torr the observed excitation functions for the ^{15}N-technique (Fig. 6a) lead to ΔE_{exp} values, which are independent of p_0: $\Delta E_{exp} = 9.72 \pm 0.15$ keV. With $\Delta E_B = 4.55$ keV and $\Delta E_{DT} = 3.67$ keV one arrives at $\Delta E_{DVR}(H_2) = 7.76 \pm 0.23$ keV, in good agreement with the expected value of 7.5 keV [5]. Excitation functions obtained for CH_4 gas (Fig. 6b) lead to the average value $\Delta E_{exp} = 11.32 \pm 0.16$ keV at $p_0 = 3.1 \times 10^{-7}$ to 4.8×10^{-6} Torr; with $\Delta E_{DT} = 1.30$ keV one finds $\Delta E_{DVR}(CH_4) = 10.28 \pm 0.23$ keV, in excellent agreement with expectation (= 10.4 keV [5]). Measurements with H_2O vapor at $p_0 \leq 6.2 \times 10^{-5}$ Torr (Fig. 6c) lead to $\Delta E_{exp} = 11.11 \pm 0.17$ keV and thus – with $\Delta E_{DT} = 1.22$ keV – to $\Delta E_{DVR}(H_2O) = 10.06 \pm 0.24$ keV (theory = 10.3 keV [5]). Finally, NH_3 gas with $p_0 \leq 7.5 \times 10^{-6}$ Torr was used (Fig. 6d): $\Delta E_{exp} = 11.43 \pm 0.19$ keV, $\Delta E_{DT} = 1.26$ keV, and $\Delta E_{DVR}(NH_3) = 10.41 \pm 0.25$ keV (theory = 10.4 keV [12]).

In summary, the results just discussed demonstrate clearly the potential and achievable precision in the observation of bond-dependent Doppler widths using the ^{15}N-technique.

7 Doppler spectroscopy of a hydrogen-terminated Si ⟨100⟩ surface

Since the Doppler broadening depends on the scalar product of the velocity vectors between projectiles and target atoms, this directional dependence could be a unique tool in the determination of H-bond directions on a solid surface, given the fact that the magnitude of the vibrational compression mode of an adsorbed H surface atom is usually much larger than that of the vibrational waggle mode. If a well-characterized single crystal is oriented at different directions with respect to the beam direction,

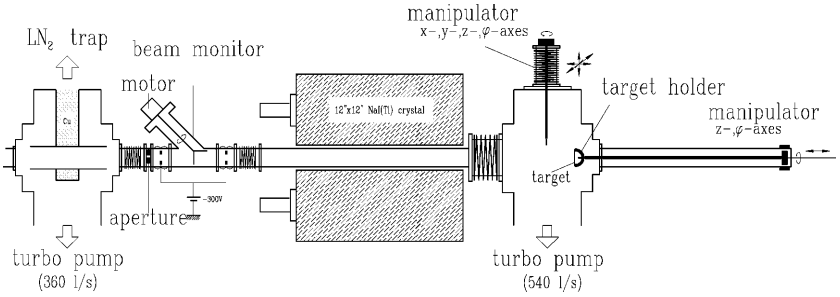

Fig. 7. Analysis chamber for the ^{15}N-technique including a 12"×12" NaI crystal and two manipulators for the transfer of samples from a transport chamber to the center of the crystal (all components built in U_{HV}-techniques). A spinning wire located upstream from the crystal was used for the measurement of ion beam current

the ^{15}N-technique should therefore reveal large vibrational Doppler widths ΔE_{DV} along directions dominated by compression mode bond vibrations and much smaller widths along directions dominated by waggle mode vibrations.

For the semiconductor industry Si crystals are of utmost importance [22]. If such a crystal is cut or cleaved, bonds are broken creating dangling bonds at the surface. The number and direction of these dangling bonds depends on the macroscopic direction of the surface normal. The surface energy is lowered by reducing the number of dangling bonds by rebounding, and this leads to a wide variety of reconstructions on Si surfaces. These dangling bonds are the source of the chemical activity of Si surfaces. If they are capped by atomic H chemisorption, the ability of the surface to react with other potential adsorbate molecules is reduced to zero. For example, a Si ⟨100⟩ surface is found to be terminated predominantly in the dihydride phase (i.e. 2 H atoms per Si surface atom) with 1.4×10^{15} H-atoms/cm^2 (= 1 monolayer) for a full surface coverage. Further, from the known vibrational frequencies [23] one expects a Doppler width of $\Delta E_{DV} = 11.5$ keV for the aligned case (i.e. the surface normal is parallel to the beam direction) and of $\Delta E_{DV} = 8.6$ keV for the random case (i.e. a polycrystalline surface). With the present energy resolution for the ^{15}N-technique such Doppler widths should be easily measurable if a well-characterized sample can be produced. However, there are inherent difficulties in the preparation of such H-bearing samples: (i) the H-bearing layer must be located on the surface of a well-ordered single crystal, (ii) the H-surface density should be 1 monolayer or less, (iii) the H atoms must be bound only to Si surface atoms (Si-H bond) and not to a mixture of contaminant bonds such as O-H and C-H, i.e. the surface must be extremely clean from contaminants at a level far below 1×10^{15} atoms/cm^2, (iv) the crystalline structure and stoichiometry of the sample should not be altered by the ambient gas in the apparatus as well as by beam-induced damage or beam-induced deposition of contaminants such as hydrocarbons. To fulfill these requirements, the apparatus for the sample preparation as well as for the sample analyses must be constructed in ultra high vacuum (U_{HV}), where the sample transport between the two equipments must also proceed under U_{HV} conditions. Furthermore, the ^{15}N-technique must be carried out with a small beam intensity (typically a few nA) in order to minimize the effects of sample damage.

Zinke-Allmang et al. [6] were the first to use the ^{15}N-technique in the study of the effects of Doppler broadening on a H random oscillator system, i.e. a hydrocarbon-laden surface. Since then, various H/solid systems (including H-Si) have been investigated, most of them representing randomly oriented H oscillators [7–10]. The most recent work of H on a Si ⟨111⟩ surface [11] produced a sample covered initially with up to 4 monolayers of hydrogen, which quickly decreased to about 1 monolayer; furthermore, no orientation effects were found and the observed value for the Doppler width lied between the expected values for ordered and random surface layers. Although the reported results [7–11] have been encouraging, a clear experimental demonstration of this vibrational Doppler spectroscopy is missing.

To elucidate further the technical requirements of the vibrational Doppler spectroscopy, we have investigated the hydrogenation of a Si ⟨100⟩ surface. For the sample preparation, a rapid thermal processing furnace – built in U_{HV} technique – was used [24, 25] to clean and hydrogenate the single crystal. The sample was then transferred via a transportable UHV chamber to the UHV analysis chamber (Fig. 7). The chamber included two manipulators to pick up the sample from the transport chamber and to transfer it to a target holder, which could move the sample to the center of the 12"×12" NaI bore-hole crystal. The target holder allowed also for two orientations of the sample normal with respect to the ion beam direction: 0° and 45°. Using the ^{15}N-technique the observed vibrational Doppler widths were $\Delta E_{DV}(0°) = 10.03 \pm 0.24$ keV and $\Delta E_{DV}(45°) = 10.12 \pm 0.23$ keV, i.e. no orientation effects were visible; the values are between the expected values for ordered and random surface layers (see above). The hydrogen content stayed constant within experimental error even after a total ^{15}N ion dose of 2×10^{16} atoms/cm^2, indicating a stable situation. However, the absolute hydrogen density corresponded to about 3.6 monolayers. It was also found that a cleaned but unhydrogenated sample showed a similar hydrogen density as a hydrogenated sample. It was concluded that the surface of the samples was seriously contaminated – probably with O-H bonds [12] – between production and analysis and that the present observations of Doppler widths made therefore no contribution to an improved understanding of the vibrational Doppler spectroscopy. The contamination occured most likely in the transport chamber, which could be maintained (during the transport between different locations) only at a pressure of about 1×10^{-8} Torr. Since the link between the transport chamber and the analysis chamber could not be baked out, a pressure of about 1×10^{-8}

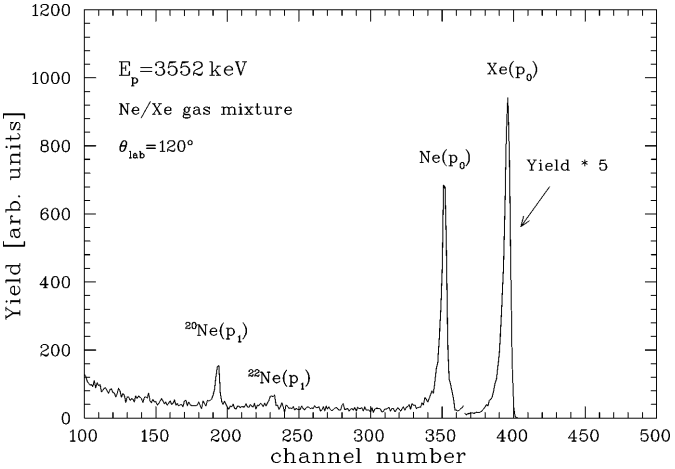

Fig. 8. Elastic scattering spectrum at $\theta_{\rm lab} = 120°$ for 3552 keV protons on a neon plus xenon gas mixture. The observed peaks are identified

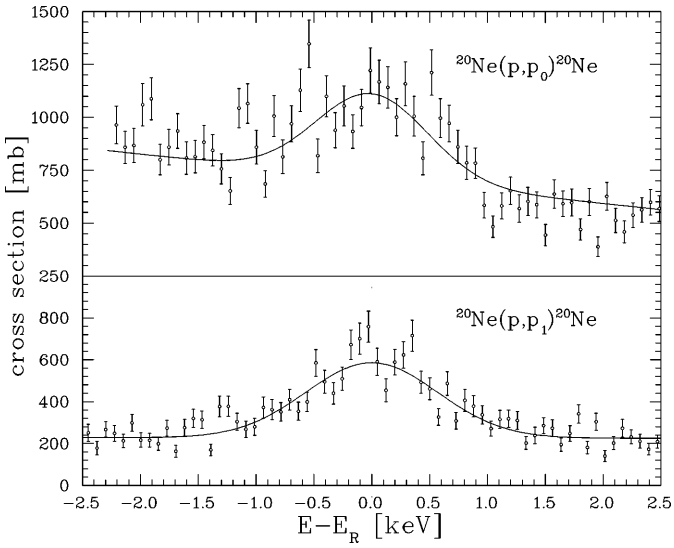

Fig. 9. Excitation function of the absolute cross section for the elastic and inelastic proton scattering on ^{20}Ne at the E_R = 3552 keV resonance. The solid curves through the data points represent the results of a fit

Torr could be reached only in the analysis chamber leading to another source of surface contamination. Therefore, future efforts in this research field must have an in-situ connection between the preparation and analysis chambers (without use of a transport chamber) with residual pressures of 1×10^{-10} Torr or better.

Appendix: total width of the 3552 and 6872 keV resonances in ^{20}Ne+p

For the $E_R = 3552$ keV resonance in the ^{20}Ne+p system, the following properties have been reported [15]: (i) formation by f-waves with $J^\pi = 7/2^-$, (ii) resonant yields in the p_0-, p_1-, and γ-exit channels, and (iii) total width $\Gamma_R \approx 400$ eV. If the true width lies near this value, it will be formed mainly by the partial widths of the p_0-channel (Γ_0) and p_1-channel (Γ_1), while the γ-channel (Γ_γ) contributes at most a few eV: $\Gamma_R = \Gamma_0 + \Gamma_1 + \Gamma_\gamma \approx \Gamma_0 + \Gamma_1$. Due to the f-wave formation, the p_0-channel is absent at the scattering angle $\theta_{\rm cm} = 90°$. Thus, the Si detector was installed in the disc-shaped target chamber [4] at the port $\theta_{\rm lab} \approx \theta_{\rm cm} = 120°$. A spectrum obtained at $E_R = 3552$ keV with a Ne/Xe gas mixture is shown in Fig. 8: the peaks corresponding to the elastic scattering on Ne and Xe as well as those of the inelastic scattering on ^{20}Ne and ^{22}Ne (Ne gas of natural isotopic composition was used, containing 10% ^{22}Ne) are well resolved. The number of counts for the elastic scattering on ^{20}Ne, I_0, has been corrected for the 10% contribution from ^{22}Ne. In the same notation, we use the symbol I_1 for the number of counts for the inelastic scattering on ^{20}Ne. Since the dominating Legendre-polynomial $P_2(\theta_{\rm cm})$ in the angular distributions is zero at $\theta_{\rm cm} = 120°$, the resonant intensities I_0 and I_1 should represent fairly well angle-independent information, i.e. they should be proportional to the respective total cross sections σ_0 and σ_1 of the resonance. The integrals of σ_0 and σ_1 over the energy region of the resonance are given by

$$\int \sigma_0 {\rm dE} = 0.5\lambda^2 \omega \Gamma_0 \Gamma_0 / \Gamma_R$$

and

$$\int \sigma_1 {\rm dE} = 0.5\lambda^2 \omega \Gamma_0 \Gamma_1 / \Gamma_R,$$

where λ is the DeBroglie wavelength and ω (= 4) is a statistical factor. It should be pointed out that the values of these integrals are independent of the beam energy spread. The ratio of the corresponding energy-integrated intensities I_0^* and I_1^* is given by the ratio of the above integrals and thus by

$$I_1^*/I_0^* = \Gamma_1/\Gamma_0 = \varepsilon.$$

With the experimental value of ε, the above equations e.g. for $\int \sigma_1 {\rm dE}$ lead to

$$\int \sigma_1 {\rm dE} = 0.5\lambda^2 \omega \varepsilon (1+\varepsilon^2)^{-2} \Gamma_R.$$

Thus, the value for Γ_R can be determined if the absolute value of the integral is known. With the Ne/Xe gas mixture of known partial pressures, the absolute cross section for the elastic and inelastic scattering on ^{20}Ne was determined relative to that on Xe, which follows the Rutherford scattering law at this beam energy. The resulting excitation functions (Fig. 9) lead to $\varepsilon = 1.09 \pm 0.04$ and $\Gamma_R = 455 \pm 67$ eV.

For the $E_R = 6872$ keV resonance in the ^{20}Ne+p system, the following properties have been reported [15]: (i) formation by d-waves with $J^\pi = 5/2^+$, (ii) resonant yields in the p_0-, p_1-, and γ-exit channels, and (iii) total width $\Gamma_R \leq 1200$ eV. Again, if the true width lies near this value, it will be formed mainly by the partial widths of the p_0-channel (Γ_0) and p_1-channel (Γ_1):

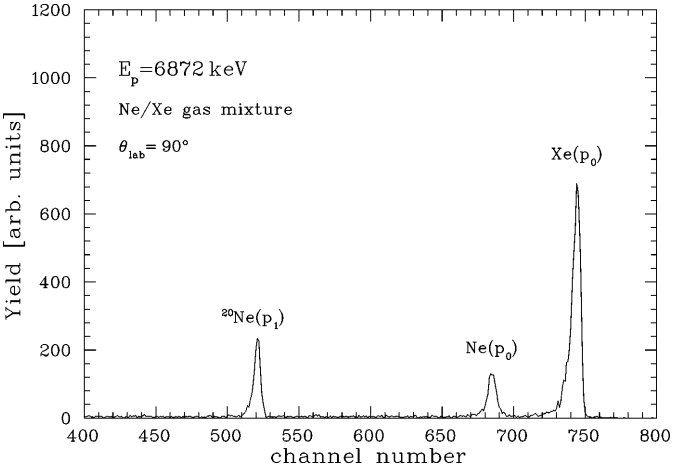

Fig. 10. Elastic scattering spectrum at $\theta_{\rm lab} = 90°$ for 6872 keV protons on a neon plus xenon gas mixture. The observed peaks are identified

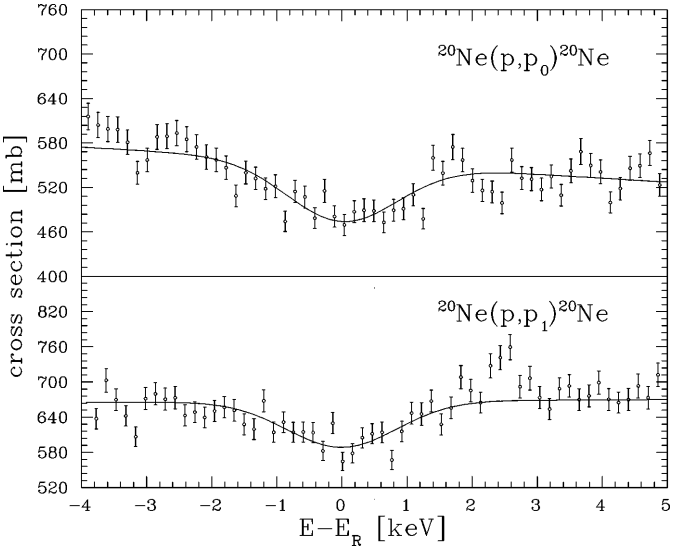

Fig. 11. Excitation function of the absolute cross section for the elastic and inelastic proton scattering on ^{20}Ne at the $E_R = 6872$ keV resonance. The solid curves through the data points represent the results of a fit

$\Gamma_R = \Gamma_0 + \Gamma_1 + \Gamma_\gamma \approx \Gamma_0 + \Gamma_1$. Due to the d-wave formation, the p_0-channel is absent at the scattering angle $\theta_{\rm cm} = 120°$. Thus, the Si detector was installed at $\theta_{\rm lab} \approx \theta_{\rm cm} = 90°$. A spectrum obtained at $E_R = 6872$ keV with a Ne/Xe gas mixture is shown in Fig. 10 and excitation functions for the elastic and inelastic scattering on ^{20}Ne in Fig. 11. Following the procedures just discussed, one finds $\varepsilon = 0.99 \pm 0.08$ and $\Gamma_R = 402 \pm 60$ eV. The small total width (corresponding to a reduced width $\Theta^2 = 1.3 \times 10^{-5}$) has its origin in the T = 3/2 isospin value of this resonance [15].

References

1. J.R. Bird, J.S. Williams: Ion Beams for Material Analysis (North Holland, 1986)
2. G. Amsel, W.A. Lanford: Ann. Rev. Nucl. Part. Sci. **34** (1984) 435
3. W.A. Lanford: Nucl. Instr. Meth. B**66** (1992) 65
4. H.W. Becker, M. Bahr, M. Berheide, L. Borucki, M. Buschmann, C. Rolfs, G. Roters, S. Schmidt, W.H. Schulte, G.E. Mitchell, J.S. Schweitzer: Z. Phys. A**351** (1995) 453
5. K.M. Horn, W.A. Lanford: Nucl. Instr. Meth. B**29** (1988) 609 and B**34** (1988) 1
6. M. Zinke-Allmang, S. Kalbitzer, M. Weiser: Z. Phys. A**325** (1986) 183
7. K. Izsak, S. Kalbitzer, M. Weiser, M. Zinke-Allmang: Nucl. Instr. Meth. B**33** (1988) 578
8. Y. Iwata, F. Fujimoto, E. Vilalta, A. Ootuko, K. Kobayashi, H. Yamashita, Y. Murata: Nucl. Instr. Meth. B**33** (1988) 574 and Jpn. J. Appl. Phys. **26** (1987) L1026
9. S. Jans, S. Kalbitzer, P. Oberschachtsiek, J.P.F. Sellschop: Nucl. Instr. Meth. B**85** (1994) 321
10. M. Zinke-Allmang, O. Kruse: Nucl. Instr. Meth. B**90** (1994) 579
11. B. Hartmann, S. Kalbitzer, M. Behar: Nucl. Instr. Meth. B**103** (1995) 494
12. L. Borucki, Thesis, Ruhr-Universität Bochum (1999)
13. H.P. Trautvetter, K. Elix, C. Rolfs, K. Brand: Nucl. Instr. Meth. **161** (1979) 173
14. S. Wüstenbecker, H.W. Becker, C. Rolfs, H.P. Trautvetter, K. Brand, G.E. Mitchell, J.S. Schweitzer: Nucl. Instr. Meth. A**256** (1987) 9
15. P.M. Endt: Nucl. Phys. A**521** (1990) 1
16. F. Ajzenberg-Selove: Nucl. Phys. A**492** (1987) 1 and A**506** (1990) 1
17. T.R. Wang, R.B. Vogelaar, R.W. Kavanagh: Phys. Rev. C**43** (1991) 883
18. W.H. Schulte, H. Ebbing, S. Wüstenbecker, H.W. Becker, M. Berheide, M. Buschmann, C. Rolfs, G.E. Mitchell, J.S. Schweitzer: Nucl. Instr. Meth. B**71** (1992) 291
19. H.A. Bethe, G. Placzek: Phys. Rev. **51** (1937) 450
20. D.S. Gemmell: Nucl. Instr. Meth. **170** (1980) 41
21. M. Mehrhoff, M. Aliotta, I.J.R. Baumvol, H.W. Becker, M. Berheide, L. Borucki, J. Domke, F. Gorris, S. Kubsky, N. Piel, G. Roters, C. Rolfs, W.H. Schulte: Nucl. Instr. Meth. B**132** (1997) 671
22. H.N. Waltenburg, J.T. Yates: Chem. Rev. **95** (1995) 494
23. L. Miglio, P. Ruggerone, G. Benedek, L. Colombo: Phys. Scripta **37** (1988) 768
24. S. Kubsky, L. Borucki, M. Berheide, S. Baier, H.W. Becker, F. Gorris, C. Grunwald, T. Gutt, G. Krüger, M. Mehrhoff, N. Piel, C. Rolfs, W.H. Schulte: Nucl. Instr. Meth. B**113** (1996) 63
25. S. Kubsky, S.A. Baier, M. Berheide, L. Borucki, F. Gorris, T. Gutt, N. Piel, C. Rolfs, W.H. Schulte, I.J.R. Baumvol, F.C. Stedile: Nucl. Instr. Meth. (to be submitted)